Boosting Rate Performance of Li–S Batteries under High-Mass-Loading Sulfur based on Hierarchical NCNT@Co-CoP Nanowires Integrated Electrode

Jianbo Li, Wenfu Xie, Shimeng Zhang, Si-Min Xu and Mingfei Shao*

State Key Laboratory of Chemical Resource Engineering, Beijing University of Chemical Technology, Beijing 100029, P. R. China.

* Email: shaomf@mail.buct.edu.cn

1. Experimental Section

Preparation of $Co(OH)_2$ nanowire arrays precursor: The $Co(OH)_2$ nanowire arrays were synthesized by a facile hydrothermal synthesis method according to previous report.[1] Typically, 5 mmol of $Co(NO_3)_2 \cdot 6H_2O$, 10 mmol of NH_4F and 25 mmol of urea were dissolved in 70 mL of deionized H_2O under ultrasonication. Then the solution was transferred into a Teflon-lined stainless-steel autoclave. A piece of nickel foam (size: 3×5×0.05 cm, pretreated with acetone, 3 M HCl solution, deionized water and ethanol each for 15 min) was immersed into the above solution. The autoclave was sealed and heated at 120 °C for 5 h, followed by cooling to room temperature naturally. The product $Co(OH)_2$ nanowire arrays were rinsed with distilled water and ethanol for several times, and dried at 60 °C for 6 h.

Preparation of NCNT@Co nanowires array: Firstly, ZIF-67 was synthesized in methanol at room temperature as previous literature. The ZIF-67 (50 mg) powder was placed in a crucible, and a piece of Ni foam (3×5×0.05 cm) supported $Co(OH)_2$ nanowire arrays is installed horizontally over the crucible. A temperature-programmed furnace was used to perform the 3D NCNT array at 800 °C and the heating rate was 5 °C min^{-1} under N_2 stream and then maintained for 2 h. The resulting product

was slowly cooled to room temperature in a N_2 stream for the subsequent use. The obtained product was named as NCNT@Co.

NCNT@Co-CoP nanowire arrays: The NCNT@Co-CoP-1 and NCNT@Co-CoP-2 NWAs were prepared by an *in-situ* phosphidation process of the NCNT@Co nanowire arrays precursor. In a typical procedure, $NaH_2PO_2 \cdot H_2O$ was adopted as phosphorus precursor, which can break into reductive PH_3. NCNT@Co were annealed in a N_2 stream at 300 °C and the heating rate was 5 °C min^{-1} under N_2 stream for 2 h. The amount of $NaH_2PO_2 \cdot H_2O$ used for phosphating NCNT@Co-CoP-1 and NCNT@Co-CoP-2 NWAs was 0.5 and 2.0 g, respectively. The resulting product was slowly cooled to room temperature in a N_2 stream.

Preparation of NCNT@Co@S, NCNT@Co-CoP-1@S and NCNT@Co-CoP-2@S cathode: The electrode is cut to a diameter of 15mm for subsequent use. Then, 100 mg S powder was dissolution into 3 mL CS_2 solution under ultrasonication. S composites electrodes were prepared by adding the above solution into the obtained NCNT@Co@S, NCNT@Co-CoP-1 and NCNT@Co-CoP-2, which further thermally treated at 155 ºC for 6 h. The areal S loading was around 4 mg cm^{-2} for regular electrodes. Meanwhile, higher S loading of 10 mg cm^{-2} were also prepared for higher energy density.

Structural characterization. SEM (Zeiss SUPRA 55) and TEM (Philips Tecnai 20 and JEOL JEM-2010 high resolution transmission electron microscopes) were performed to investigate the morphologies and microstructures of the obtained samples. The XRD patterns were collected on a Shimadzu XRD-6000 diffractometer using a Cu Kα source, with a scan range between 3° and 70° at a scanning speed of 10° min^{-1}. The Raman spectrometry was performed with Renishaw, in Via-Reflex, 532 nm. XPS spectra were collected on a Thermo VG ESCALAB 250 X-ray photoelectron spectrometer at a pressure of about 2×10^{-9} Pa using Al Kα X-rays as the excitation source. The UV–

vis absorption spectra were measured on a UV–vis spectrophotometer (UV-2450, Japan) within the wavelength range of 200–500 nm.

Adsorption Tests: The Li_2S_6 solution (5 mM) was prepared by mixing the Li_2S and sublimed S with a molar ratio of 1 : 5 in DOL /DME (1:1 by volume) under stirring at 60 °C for continuous stirring for 24 h in a glove box. The NCNT@Co@S, NCNT@Co-CoP-1 and NCNT@Co-CoP-2 samples with the similar size were immersed into Li_2S_6 solution to ensure fully adsorption. Digital images were taken after resting for 12 h. Afterwards, the supernatant solution was collected for the analysis by a UV-vis spectrometer.

Symmetric Cell Measurements: The symmetrical cells were assembled by using the obtained electrodes as both cathode and anode with the electrolyte containing 0.5 M Li_2S_6. The CV curves of the symmetrical cells were recorded at a scanning rate of 5 mV s^{-1} in the potential range of −1.0 to 1.0 V.

Electrochemical Measurements. The CR2032 coin cells were assembled by using S composite electrode as cathode, Celguard 2400 as the separator, and Li metal anode as the counter electrode in an argon-filled glovebox. The electrolyte contains 1 M lithium bis(trifluoromethane) sulfonamide (LiTFSI) in a binary solvent of dimethoxymethane/1,3-dioxolane (DME/DOL, 1:1 by volume) with 2 wt.% $LiNO_3$ as additive. The size of Li metal anode, separator, and cathode electrode were 15.6, 16.0 and 15.0 mm in diameter, respectively. The S areal loadings were ~4 mg cm^{-2} for normal cathodes and ~10 mg cm^{-2} for high-loading cathodes. The ratio of electrolyte to S was 15 μL mg^{-1} for normal cathodes and 7 μL mg^{-1} for high-loading cathodes. Cyclic voltammetry (CV) and EIS study (0.1 Hz to 100k Hz with an amplitude of 5 mV) were carried out on a CHI660E electrochemical workstation (Shanghai Chenhua Instrument Co, China). The cells were galvanostatically charged and discharged

between 1.7 and 2.8 V versus Li/Li^+ at various current densities on a LAND test system at room temperature. The current density and specific capacity are calculated based on the mass of S.

***In Situ* Raman Spectroscopy.** *In situ* Li−S batteries tank with a quartz window were used for the in-situ Raman spectroscopy analysis. The conditions for assembling the battery are consistent with the button battery. The batteries were run at a (dis)charge rate of 0.1 C (1 C = 1675 mAh g^{-1}). Raman signals were simultaneously recorded every 10 min during the (dis)charging cycling of the Li−S batteries.

Model construction. The model of bulk Co was built according to the experimental X-ray diffraction data.[2] The space group of bulk Co is $Fm\bar{3}m$, with the lattice parameters of $a = b = c = 3.544$ Å, $\alpha = \beta = \gamma = 90^\circ$. Then, the model of Co was built by cleaving the (111) facet of bulk Co, containing four layers of Co atoms and vacuum layer of 15 Å. The supercell of Co was 6 × 4 in *a*-, and *b*- directions. Therefore, the chemical formula of model Co was Co_{96}.

The model of bulk CoP was built according to the experimental X-ray diffraction data.[3] The space group of bulk CoP was Pbnm, with the lattice parameters of $a = 5.599$ Å, $b = 5.076$ Å, $c = 3.281$ Å, $\alpha = \beta = \gamma = 90^\circ$. Then, the model of CoP was built by cleaving the (111) facet of bulk CoP, containing four layers of Co atoms, four layers of P atoms, and vacuum layer of 15 Å. The supercell of CoP was 2 × 2 in *a*-, and *b*- directions. Therefore, the chemical formula of model CoP was $Co_{32}P_{32}$.

The model of Co-CoP was constructed by integrating four layers of Co and two layers of CoP into one cell with the lattice parameters of $a = 15.115$ Å, $b = 12.088$ Å, $c = 34.895$ Å, $\alpha = \beta = 90^\circ$, $\gamma = 124.3^\circ$. The chemical formula of model Co-CoP was $Co_{128}P_{32}$.

Computational method. The spin-polarized density functional theory (DFT) calculations at generalized gradient approximation (GGA) Perdew-Burke-Ernzerhof (PBE) level were performed

with Cambridge Sequential Total Energy Package.[4] The ionic cores were described with the ultrasoft pseudopotentials and the cutoff energy was set as 300 eV. The geometry optimization was based on the following 3 points: (a) an energy tolerance of 1×10^{-5} eV/atom, (b) a maximum displacement tolerance of 1×10^{-3} Å, and (c) a force tolerance of 0.03 eV/Å.

The binding energy between LiPS (Li_2S_4, Li_2S_6, and Li_2S_8) and electrode (Co, Co-CoP, and CoP, denoted as *) was calculated with eq 1,

$$E_B = E_* + E_{LiPS} - E_{LiPS*} \quad (1)$$

where E_*, E_{LiPS}, and E_{LiPS*} represented the energy of *, LiPS, and LiPS*, respectively.

The diffusion pathway of Li^+ was defined to be starting from the optimal adsorption site of Li^+, to adjacent optimal adsorption site. Take Co for example, the optimal adsorption site for Li^+ on Co was calculated to be the bridge site. After that, the energy evolution along the diffusion pathway was calculated. The energy difference between the highest energy and the lowest energy in diffusion pathway was defined as the diffusion barrier.

2. Supplementary Figures and Tables

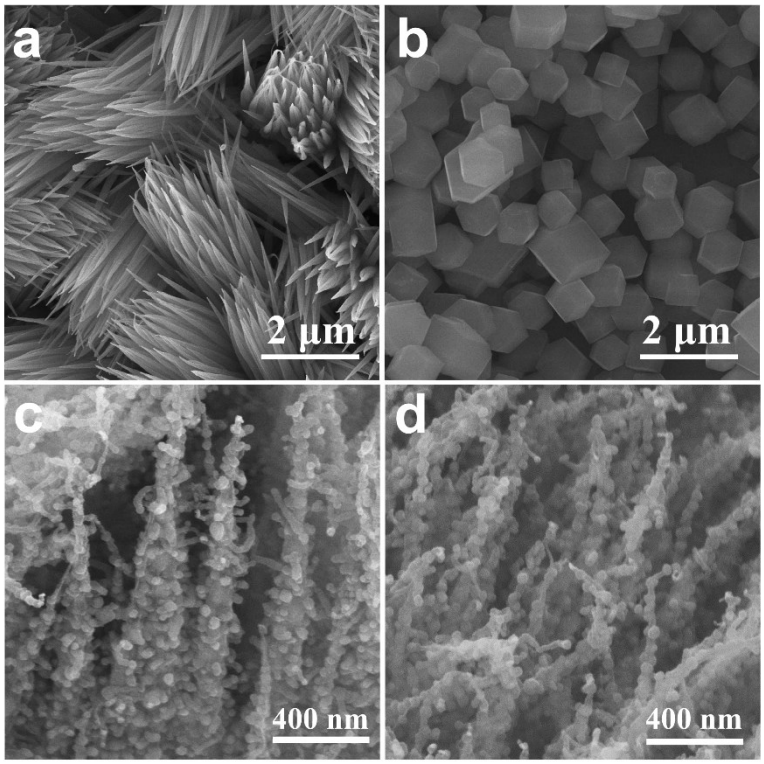

Fig. S1. SEM images of (a) $Co(OH)_2$, (b) ZIF-67, (c) NCNT@Co and (d) NCNT@Co-CoP-2, respectively.

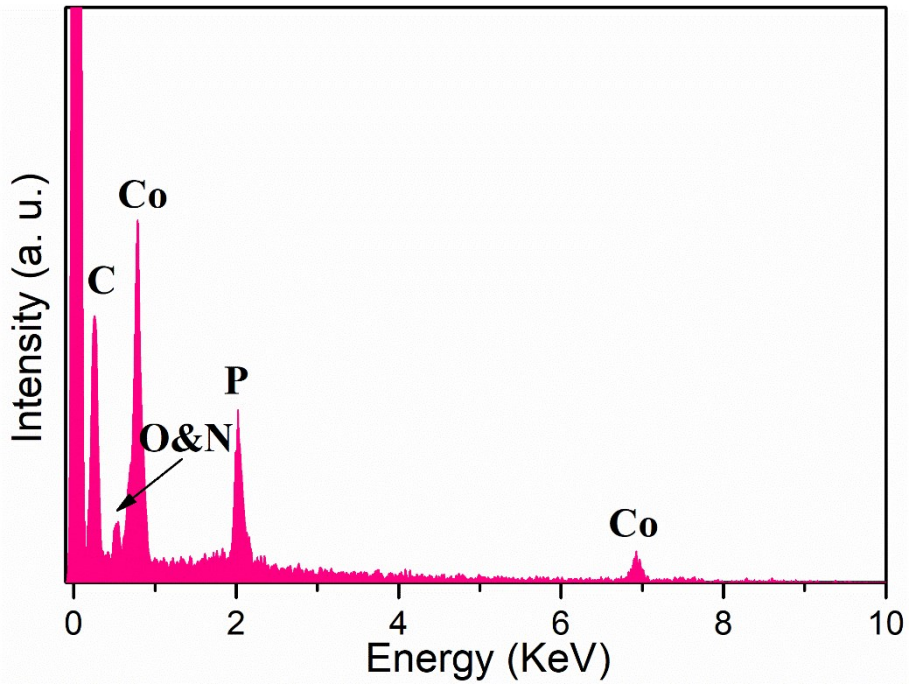

Fig. S2. SEM-EDX of the NCNT@Co-CoP-1.

Table S1. The composition for NCNT@Co-CoP-1 from EDS result

Element	Atomic%
C	66.22
N	4.31
O	4.74
P	6.50
Co	18.23

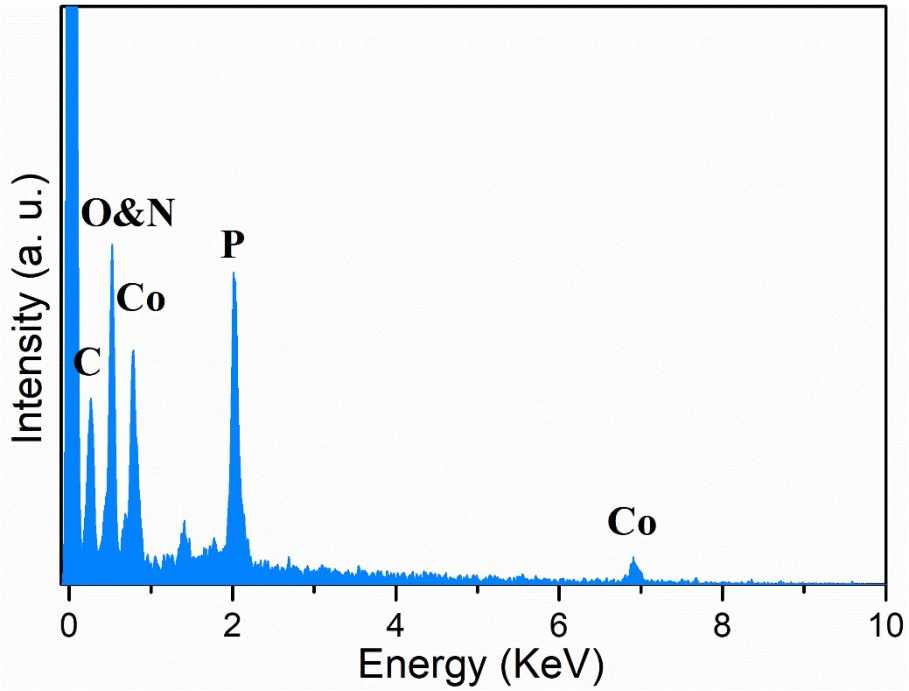

Fig. S3. SEM-EDX of the NCNT@Co-CoP-2.

Table S2. The composition for NCNT@Co-CoP-2 from EDS result

Element	Atomic%
C K	48.70
N K	2.95
O K	24.76
P K	11.52
Co L	12.08

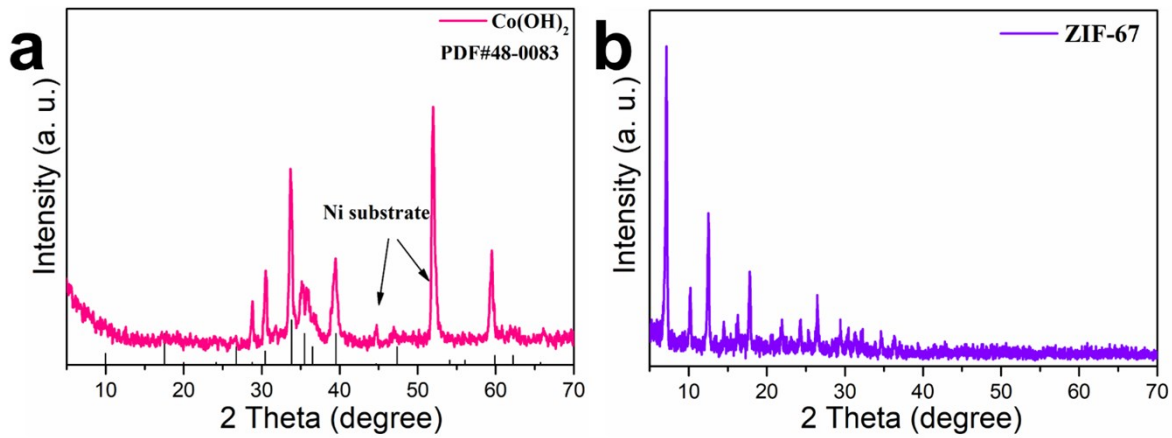

Fig. S4. XRD of (a) $Co(OH)_2$ and (b) ZIF-67.

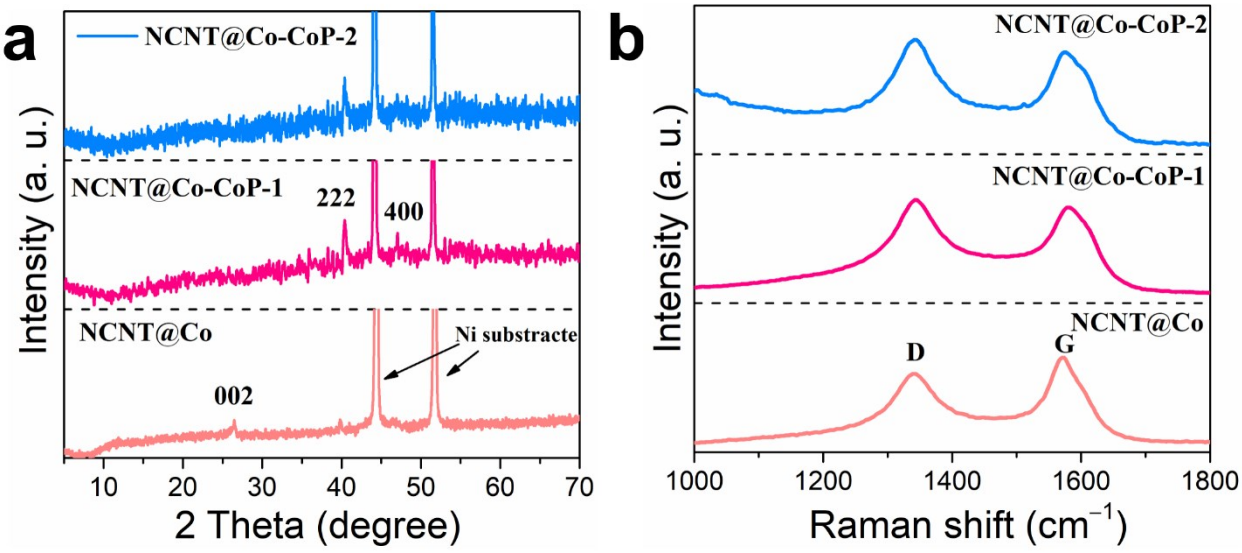

Fig. S5. (a) XRD patterns (b) Raman spectra of NCNT@Co, NCNT@Co-CoP-1 and NCNT@Co-CoP-2, respectively.

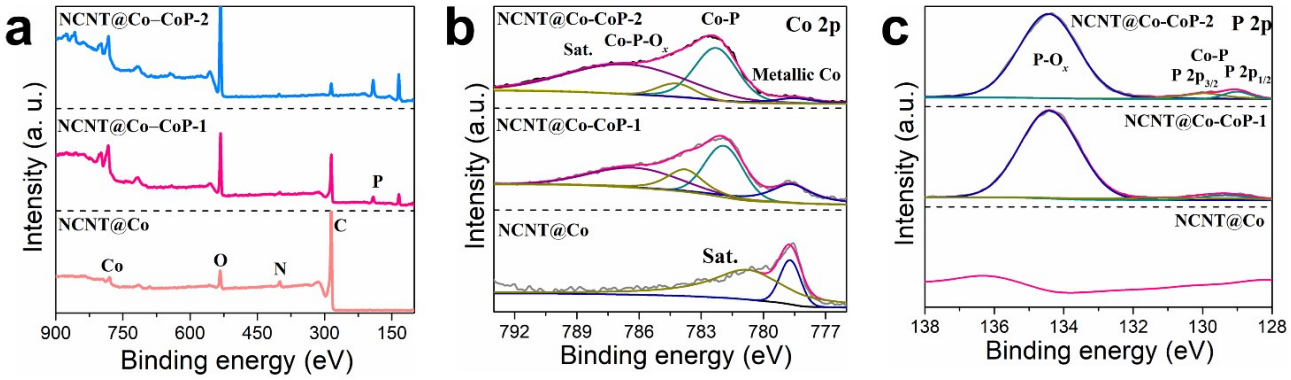

Fig. S6. (a) Full survey of XPS spectra and high resolution XPS spectra of (b) Co 2p, (c) P 2p for NCNT@Co, NCNT@Co-CoP-1 and NCNT@Co-CoP-2, respectively.

.

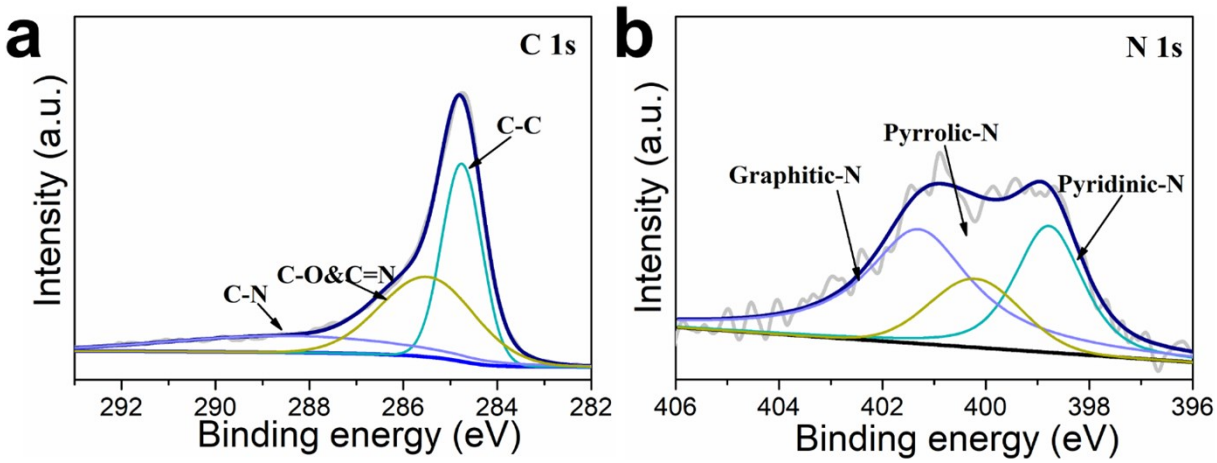

Fig. S7. high resolution XPS spectra of (a) C 1s and (b) N 1s for NCNT@Co-CoP-1.

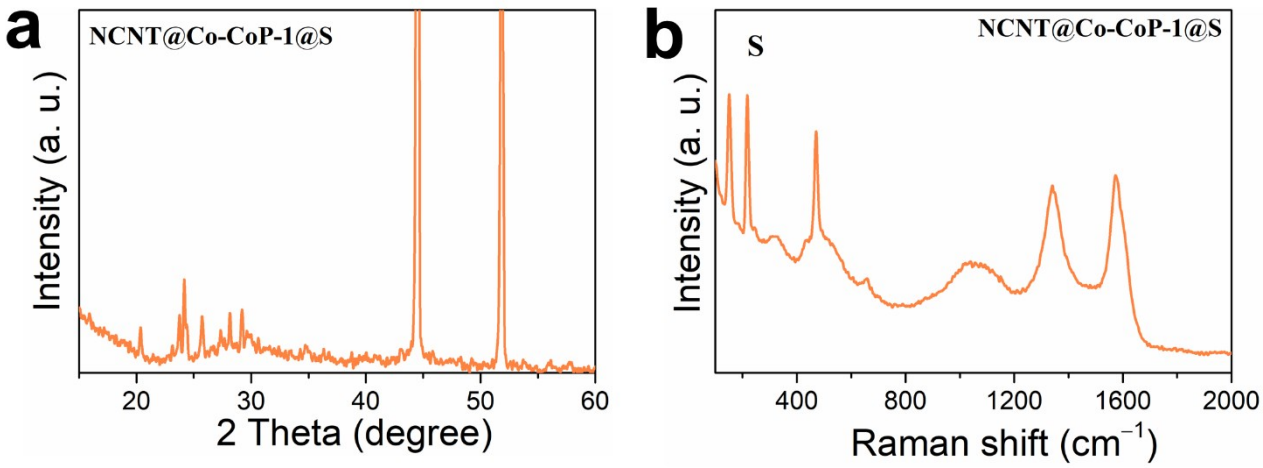

Fig. S8. (a) XRD patterns (b) Raman spectra of NCNT@Co-CoP-1@S respectively.

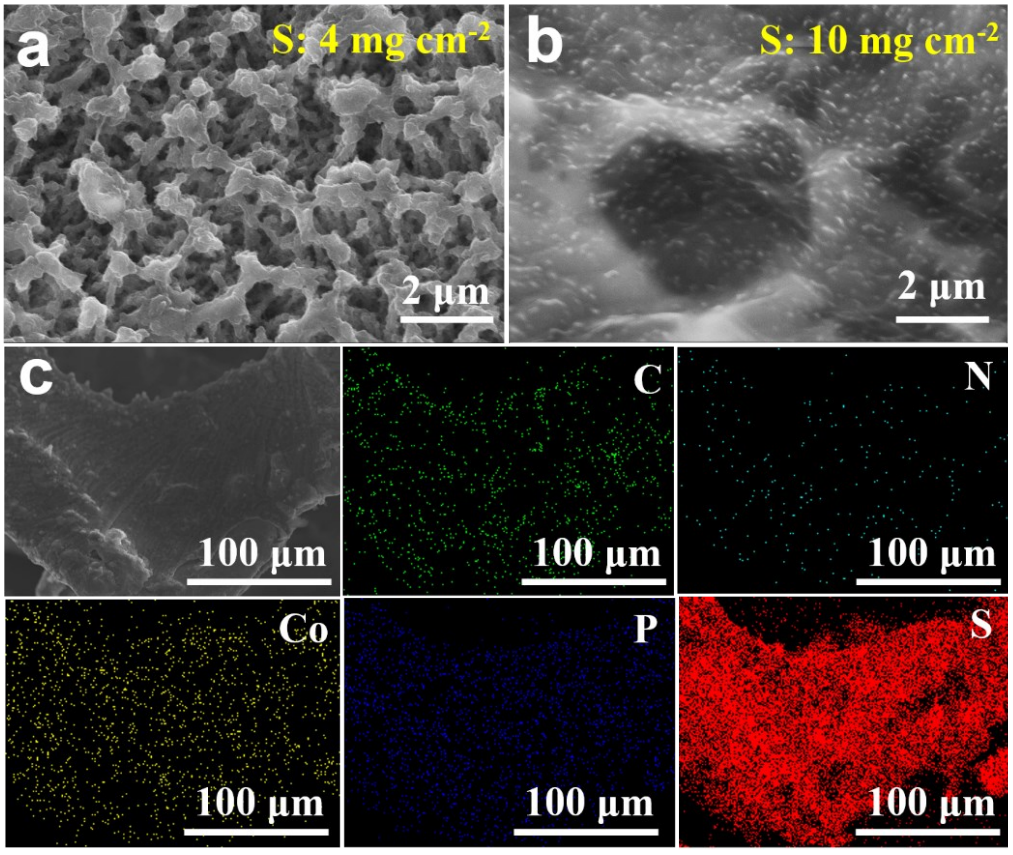

Fig. S9. SEM images NCNT@Co-CoP-1@S cathode with S loading of (a) 4 and (b) 10 mg cm^{-2}, respectively. (c) The elemental mappings of NCNT@Co-CoP-1@S cathode with S loading of 10 mg cm^{-2}.

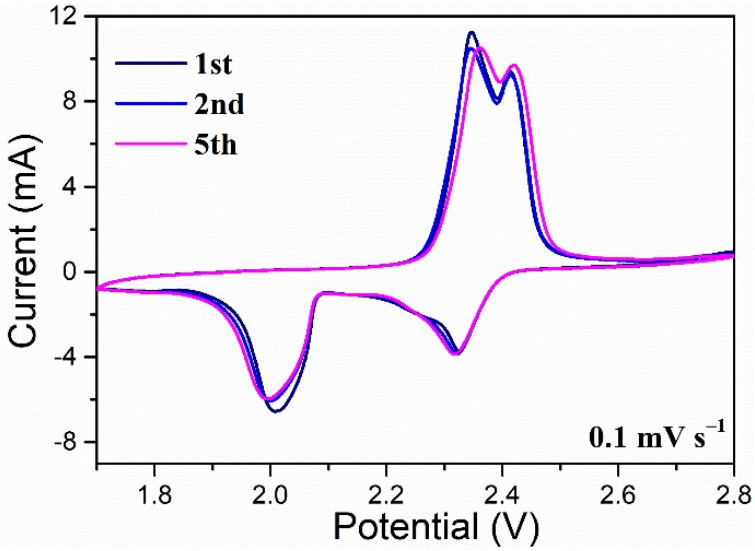

Fig. S10. CVs of NCNT@Co-CoP-1@S in Li−S batteries at a scan rate of 0.1 mV s^{-1} between 1.7 and 2.8 V.

Table S3. The performance comparison between NCNT@Co-CoP-1@S and recently reported S electrodes

Cathode material	**Mass loading (S mg cm^{-2})**	**Cycling stability**
NCNT@Co-CoP-1@S	**~4.0**	**603.8 mAh g^{-1} after 900 cycles at 5 C**
S@ZnSe/NHC[5]	~1.0	658 mAh g^{-1} after 800 cycles at 1 C
3D S-VN@N-PGC[6]	~1.0	466 mAh g^{-1} after 1700 cycles at 2 C
C@TiN-S[7]	~1.1	453 mAh g^{-1} after 300 cycles at 3 C
WCNP@HCPC–S[8]	~1.2	568 mAh g^{-1} after 500 cycles at 5 C
TiC@C-TiO_2[9]	~1.2–1.6	313 mAh g^{-1} after 1000 cycles at 2 C

CoP@N-C[10]	~1.5	918 mAh g^{-1} after 500 cycles at 1 C
S/VTe_2@MgO[11]	~1.5	~552 mAh g^{-1} after 500 cycles at 2 C
Mo-N-C/S[12]	~2.0	743.9 mAh g^{-1} after 550 cycles at 5 C
3DOM Nb_2O_{5-x}/CNTs[13]	~2.0	847 mAh g^{-1} after 500 cycles at 1 C
VN-550[14]	~2.5	847 mAh g^{-1} after 400 cycles at 2 C
S/N-CN-750@Co_3Se_4[15]	~3.1	531 mAh g^{-1} after 800 cycles at 0.2 C
MoB/S[16]	~3.2	600 mAh g^{-1} after 1000 cycles at 1 C
CS@HPP[17]	~3.7	414.3 mAh g^{-1} after 1200 cycles at 2 C
$Ti_3C_2T_x$@S/CC[18]	~4.0	746.1 mAh g^{-1} after 200 cycles at 1 C
S@Mn/C-(N, O)[19]	~4.0	525 mAh g^{-1} after 1000 cycles at 1 C
h-Co_4N@NC/S[20]	~4.5	658 mAh g^{-1} after 400 cycles at 5 C

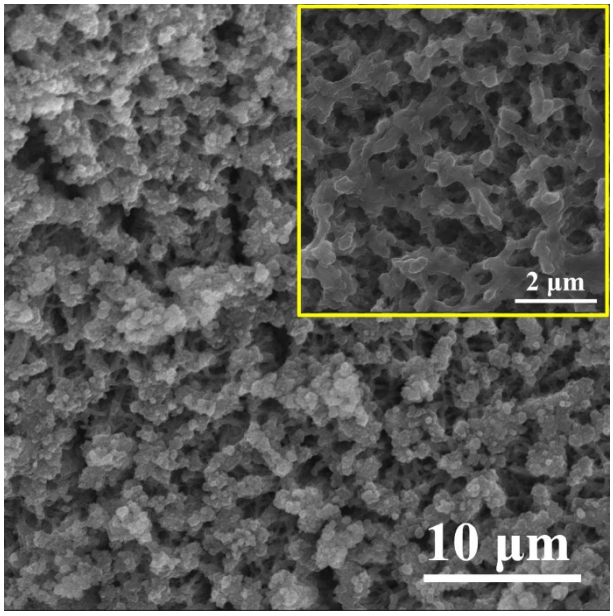

Fig. S11. SEM images of NCNT@Co-CoP-1@S cathode after 150 cycles at 1 C.

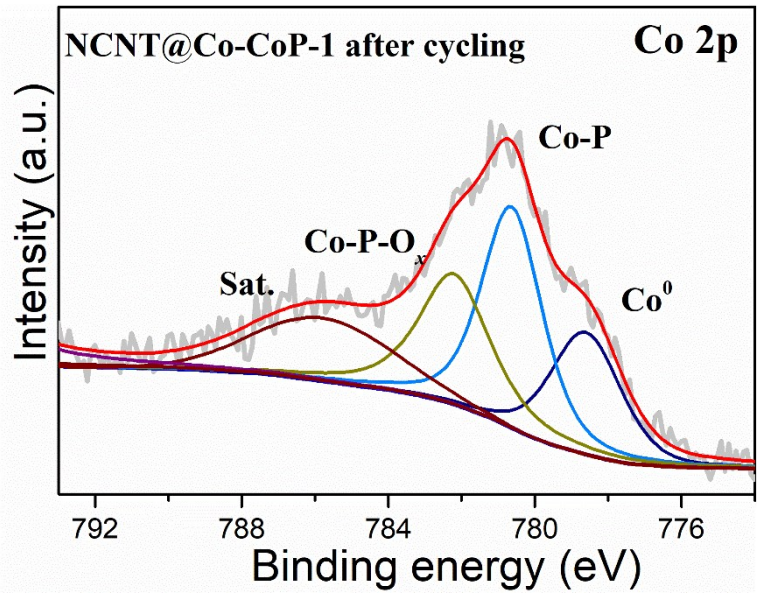

Fig. S12. XPS spectra of Co 2p for NCNT@Co-CoP-1 after cycling.

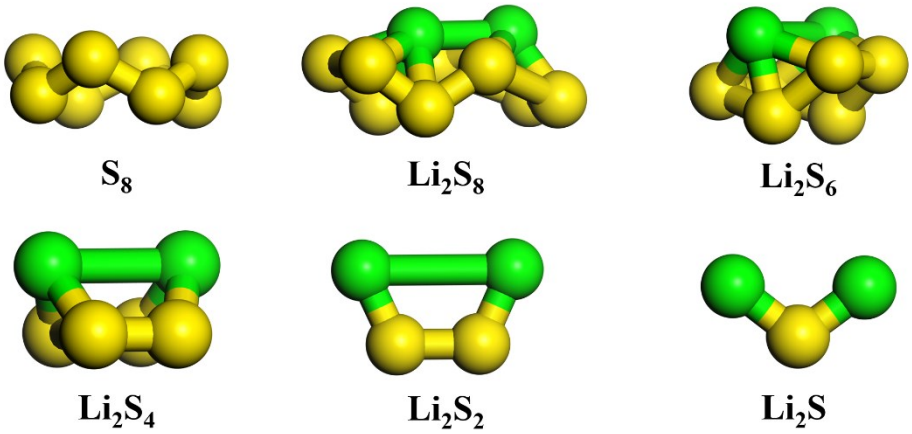

Fig. S13. Optimized geometries of S species.

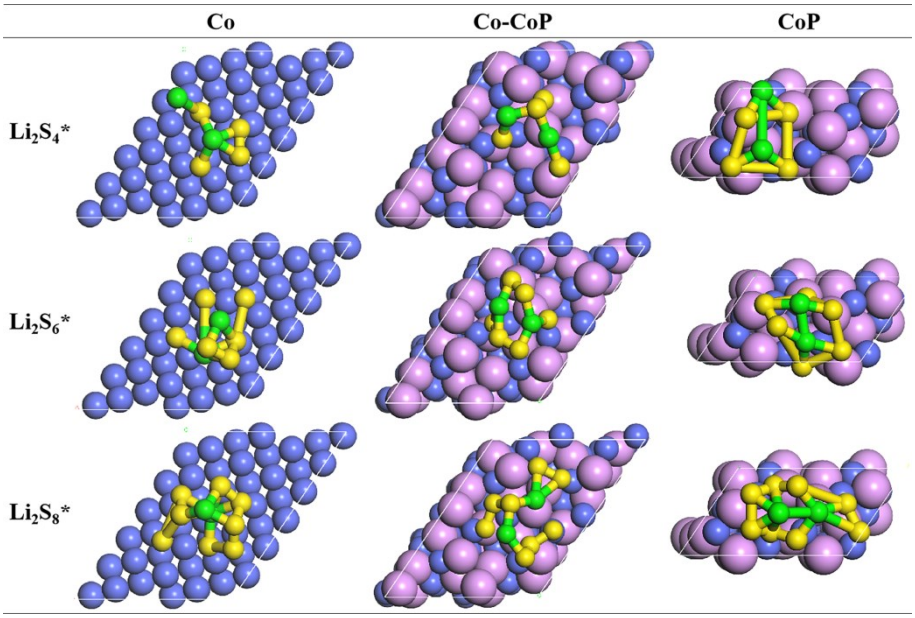

Fig. S14. Optimized geometries of LiPSs (Li_2S_4, Li_2S_6, and Li_2S_8) adsorbed on Co, Co-CoP, and CoP.

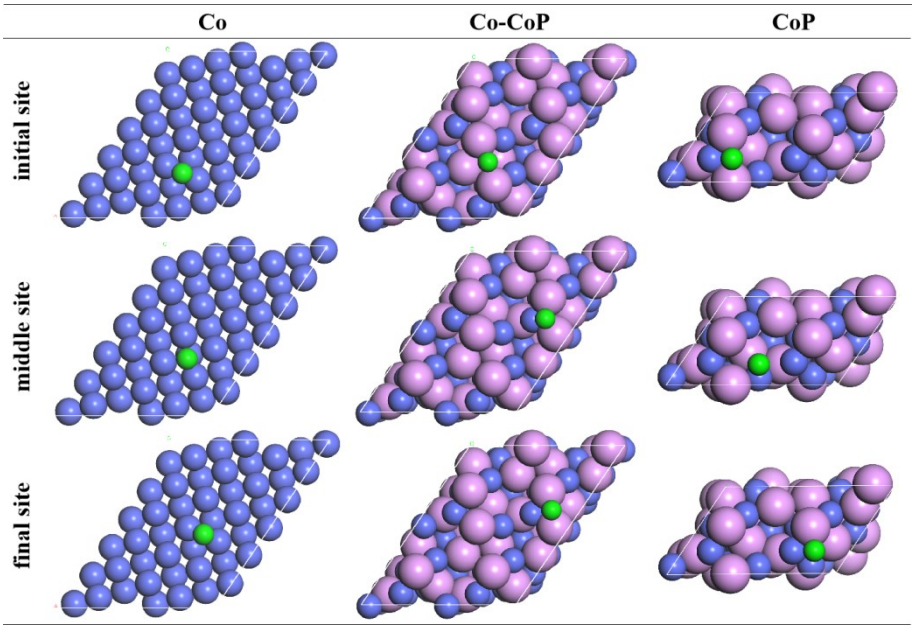

Fig. S15. Optimized geometries of Li^+ adsorbed at the initial, middle, and final sites in the diffusion pathway on Co, Co-CoP, and CoP.

3. References

1 F. Y. Ning, M. F. Shao, C. L. Zhang, S.-M. Xu, M. Wei, X. Duan, *Nano Energy*, 2014, **7**, 134−142.

2 A. Taylor, R. W. Floyd, *Acta Crystallogr.*, 1950, **3**, 285–289.

3 R. W. G. Wyckoff, *Cryst. Struct*., 1963, **1**, 85–237.

4 S. J. Clark, M. Segall, C. J. Pickard, P. J. Hasnip, *Zeitschrift Fur. Kristallographie*, 2005, **220**, 567–570.

5 D. W. Yang, C. Q. Zhang, J. J. Biendicho, X. Han, Z. F. Liang, R. F. Du, M. Y. Li, J. S. Li, J. Arbiol, J. Llorca, Y. T. Zhou, J. R. Morante, A. Cabot, *ACS Nano*, 2020,**14**, 15492–15504.

6 X. Y. Yang, S. Chen, W. B. Gong, X. D. Meng, J. P. Ma, J. Zhang, L. R. Zheng, H. D. Abruña, J. X. Geng, *Small*, 2020, **16**, 2004950.

7 Y. K. Wang, R. F. Zhang, Y.-C. Pang, X. Chen, J. X. Lang, J. J. Xu, C. H. Xiao, H. L. Li, K. Xi, S. J. Ding, *Energy Stor. Mater.*, 2019, **16**, 228–235.

8 J. Zhang, S. R. Duan, C. Y. You, J. Wang, H. T. Liu, S. H. Guo, W. H. Zhang, R. Yang, *J. Mater. Chem. A*, 2020, **8**, 22240–22250.

9 X. Q. Zhang, W. Yuan, Y. Yang, Y. Chen, Z. H. Tang, C. Wang, Y. H. Yuan, Y. T. Ye, Y. P. Wu, Y. Tang, *Small* 2020, 2005998.

10 Q. Cheng, Z. H. Yin, S. Y. Pan, G. Z. Zhang, Z. X. Pan, X. Y. Yu, Y. P. Fang, H. S. Rao, X. H. Zhong, *ACS Appl. Mater. Interfaces*, 2020, **12**, 43844–43853.

11 M. L. Wang, Y. Z. Song, Z. T. Sun, Y. L. Shao, C. H. Wei, Z. Xia, Z. N. Tian, Z. F. Liu, J. Y. Sun, *ACS Nano*, 2019, **13**, 13235−13243.

12 F. Ma, Y. Y. Wan, X. M. Wang, X. C. Wang, J. S. Liang, Z. P. Miao, T. Y. Wang, C. Ma, G. Lu, J. T. Han, Y. H. Huang, Q. Li, *ACS Nano*, 2020, **14**, 10115−10126.

13 J. Y. Wang, G. R. Li, D. Luo, Y. G. Zhang, Y. Zhao, G. F. Zhou, L. L. Shui, X. Wang, Z. W. Chen, *Adv. Energy Mater*., 2020, **10**, 2002076.

14 S. S. Tan, Y. H. Dai, Y. L. Jiang, Q. L. Wei, G. B. Zhang, F. Y. Xiong, X. Q. Zhu, Z.-Y. Hu, L. Zhou, Y. C. Jin, K. Kanamura, Q. Y. An, L. Q. Mai, *Adv. Funct. Mater.*, 2020, 2008034.

15 D. Cai, B. K. Liu, D. H. Zhu, D. Chen, M. J. Lu, J. M. Cao, Y. H. Wang, W. H. Huang, Y. Shao, H. R. Tu, W. Han, *Adv. Energy Mater.*, 2020, **10**, 1904273.

16 J. R. He, A. Bhargav, A. Manthiram, *Adv. Mater*., 2020, 2004741.

17 Z. Q. Ye, Y. Jiang, L. Li, F. Wu, R. J. Chen, *Adv. Mater.*, 2020, **32**, 2002168.

18 F. Yin, Q. Jin, H. Gao, X. T. Zhang, Z. G. Zhang, *J. Energy Chem.*, 2021, **53**, 340–346.

19 Y. N. Liu, Z. Y. Wei, B. Zhong, H. T. Wang, L. Xia, T. Zhang, X. M. Duan, D. C. Jia, Y. Zhou, X. X. Huang, *Energy Stor. Mater.*, 2021, **35**, 12–18.

20 Z. X. Sun, S. Vijay, H. H. Heenen, A. Y. S. Eng, W. G. Tu, Y. X. Zhao, S. W. Koh, P. Q. Gao, Z. W. Seh, K. Chan, H. Li, *Adv. Energy Mater*., 2020, **10**, 1904010.